Naval Research Laboratory

Washington, DC 20375-5320

NRL/MR/8221--18-9834

Discontinuous-Galerkin Simulations of Premixed Ethylene-Air Combustion in a Cavity Combustor

Gabriel B. Goodwin, Ryan F. Johnson, Andrew T. Corrigan and Andrew D. Kercher

Space Mechanical Systems Development Branch
Spacecraft Engineering Department

Month 00, 2019

DISTRIBUTION STATEMENT A: Approved for public release; distribution is unlimited.

REPORT DOCUMENTATION PAGE

Form Approved
OMB No. 0704-0188

Public reporting burden for this collection of information is estimated to average 1 hour per response, including the time for reviewing instructions, searching existing data sources, gathering and maintaining the data needed, and completing and reviewing this collection of information. Send comments regarding this burden estimate or any other aspect of this collection of information, including suggestions for reducing this burden to Department of Defense, Washington Headquarters Services, Directorate for Information Operations and Reports (0704-0188), 1215 Jefferson Davis Highway, Suite 1204, Arlington, VA 22202-4302. Respondents should be aware that notwithstanding any other provision of law, no person shall be subject to any penalty for failing to comply with a collection of information if it does not display a currently valid OMB control number. **PLEASE DO NOT RETURN YOUR FORM TO THE ABOVE ADDRESS.**

1. REPORT DATE *(DD-MM-YYYY)*
20-12-2018

2. REPORT TYPE
Memorandum Report

3. DATES COVERED *(From - To)*
April - September 2018

4. TITLE AND SUBTITLE

Discontinuous-Galerkin Simulations of Premixed Ethylene-Air Combustion in a Cavity Combustor

5a. CONTRACT NUMBER

5b. GRANT NUMBER

5c. PROGRAM ELEMENT NUMBER

6. AUTHOR(S)

Gabriel B. Goodwin, Ryan F. Johnson, Andrew T. Corrigan and Andrew D. KERCHER

5d. PROJECT NUMBER

5e. TASK NUMBER

5f. WORK UNIT NUMBER
82-1J09-08

7. PERFORMING ORGANIZATION NAME(S) AND ADDRESS(ES)

Naval Research Laboratory
4555 Overlook Avenue, SW
Washington, DC 20375-5344

8. PERFORMING ORGANIZATION REPORT NUMBER

NRL/MR/8221--18-9834

9. SPONSORING / MONITORING AGENCY NAME(S) AND ADDRESS(ES)

10. SPONSOR / MONITOR'S ACRONYM(S)

11. SPONSOR / MONITOR'S REPORT NUMBER(S)

12. DISTRIBUTION / AVAILABILITY STATEMENT

DISTRIBUTION STATEMENT A: Approved for public release; distribution is unlimited.

13. SUPPLEMENTARY NOTES

14. ABSTRACT

One of the primary challenges in design of a robust scramjet engine is minimizing combustor length, and consequently internal drag, while maintaining adequate residence time for mixing and complete combustion. The cavity ameholder increases residence time by inducing a recirculating flow suitable for sustained combustion in a scramjet engine. An additional benefit to this conguration is that the total pressure losses are low compared to that observed in other ameholders. Experiments at the University of Virginia Supersonic Combustion Facility have investigated combustion of premixed ethylene-air with a cavity ameholder. In this paper, the Naval Research Laboratory's high delity Discontinuous-Galerkin code, JENRE, is used to simulate combustion in this facility. The primary goal of this work is to use these simulations to enhance our understanding of fully premixed, dual-mode scramjet combustion with a hydrocarbon fuel. A secondary goal is to compare the experimental results with those of the simulation for the purpose of validating the high-order numerical solutions to the reactive Navier-Stokes equations.

15. SUBJECT TERMS

16. SECURITY CLASSIFICATION OF:			**17. LIMITATION OF ABSTRACT**	**18. NUMBER OF PAGES**	**19a. NAME OF RESPONSIBLE PERSON**
					Gabriel B. Goodwin
a. REPORT	**b. ABSTRACT**	**c. THIS PAGE**	Unclassified Unlimited	16	**19b. TELEPHONE NUMBER** *(include area code)*
Unclassified Unlimited	Unclassified Unlimited	Unclassified Unlimited			(202) 404-2710

Standard Form 298 (Rev. 8-98)
Prescribed by ANSI Std. Z39.18

This page intentionally left blank.

Contents

1 Introduction 1

2 Experimental Configuration & Computational Geometry 2

3 Numerical Model 3
3.1 The Discontinuous Galerkin Discretization 5
3.2 Temporal Integration 6

4 Results 6
4.1 Three Step Model 6
4.2 117 Step Model 6

5 Discussion 11

6 Conclusions 12

This page intentionally left blank.

1 Introduction

Maintaining flame stability with a high combustion efficiency in dual-mode scramjet engines becomes a challenge for flight Mach numbers of 4–6, as residence time in the combustor approaches the ignition delay of the fuel-air mixture. The option to increase the combustor length to allow for longer residence times is not viable for compact vehicles. Additionally, the thrust-to-drag ratio is approximately proportional to the diameter-to-length ratio of the combustor, resulting in increasing internal drag and total pressure loss with combustor length. An alternative to lengthening the combustor is to introduce regions of recirculation within the combustor through the use of a cavity flameholder. The shear layer that forms at the leading edge of the cavity results in recirculation of the fuel-air mixture in the cavity that increases residence time and enhances combustion completeness [1].

Experiments comparing combustors with and without cavities found faster mixing, enhanced volumetric heat release, and greater recovery temperature in cavity combustors, though these metrics were also dependent on flow conditions and cavity geometry [2]. Oscillations in flame location and heat release have been observed to occur in cavity combustors [3], due to intrinsic fluid instabilities resulting from cavity and injection configuration, though these oscillations can be reduced or eliminated through cavity design. Cavity-type combustors have been demonstrated to be very effective at flame stabilization using hydrocarbon fuels at a wide range of operating conditions and fuel-air equivalence ratios for flight Mach numbers of 4–6 [4], a regime of interest for dual-mode scramjet engines.

The dual-mode, direct-connect combustor at the University of Virginia Supersonic Combustion Facility (UVASCF), shown in Fig. 1, is used to study combustion of premixed ethylene and air at flight enthalpies up to Mach 5 (stagnation temperature of 1200 K). The UVASCF combustor is the first in reported literature to successfully operate with a stable, cavity anchored flame in premixed fuel-air mode for long durations with highly repeatable results [5]. Recent experiments using planar laser-induced fluorescence (PLIF) [6], particle image velocimetry (PIV) [7], and coherent anti-Stokes Raman spectroscopy (CARS) [8], have provided detailed measurements and visualizations of subsonic combustion in the UVASCF.

A computational study conducted by Ramesh et al. [9] used a Large Eddy Simulation/Reynolds-Averaged Navier Stokes (LES/RANS) method to simulate subsonic combustion in the UVASCF, finding large-scale oscillations in heat release, pressure, and mass flowrate. A subsequent expansion of this study [10] found that the LES/RANS simulation results were highly sensitive to boundary conditions. The oscillations observed in the prior study were eliminated by raising the wall temperature in the combustor and the simulations showed good correlation with experimental results. Subsonic combustion in the UVASCF has also recently been simulated using direct numerical simulation [11], comparing the existing combustor configuration, with a ramp at the downstream end of the cavity, to a cavity without a ramp. The ramp cavity suppressed unsteady oscillations within the combustor by preventing unsteady vortex shedding at the downstream edge of the cavity.

In this paper, we present simulations of premixed ethylene-air combustion in the UVASCF in order to assess the ability of the cavity-ramp flameholder to stabilize a premixed flame. The computations will be performed using JENRE, the Naval Research Laboratory's high-order Discontinuous Galerkin code for solving the unsteady, reactive Navier-Stokes equations. Two chemical models are used for ethylene-air combustion: a 117 step, 26 species model reduced from the Jetsurf 2.0 model [12] and a three step, six species model as described in [13]. Two-dimensional (2D) simulations were performed with both of these models and the results compared with one another and experiments. The experimental configuration is detailed in Sec. 2. Section 3 describes the numerical methodology used in the simulations, the simulation results are presented in Sec. 4, followed by conclusions in

Manuscript approved December 20, 2018.

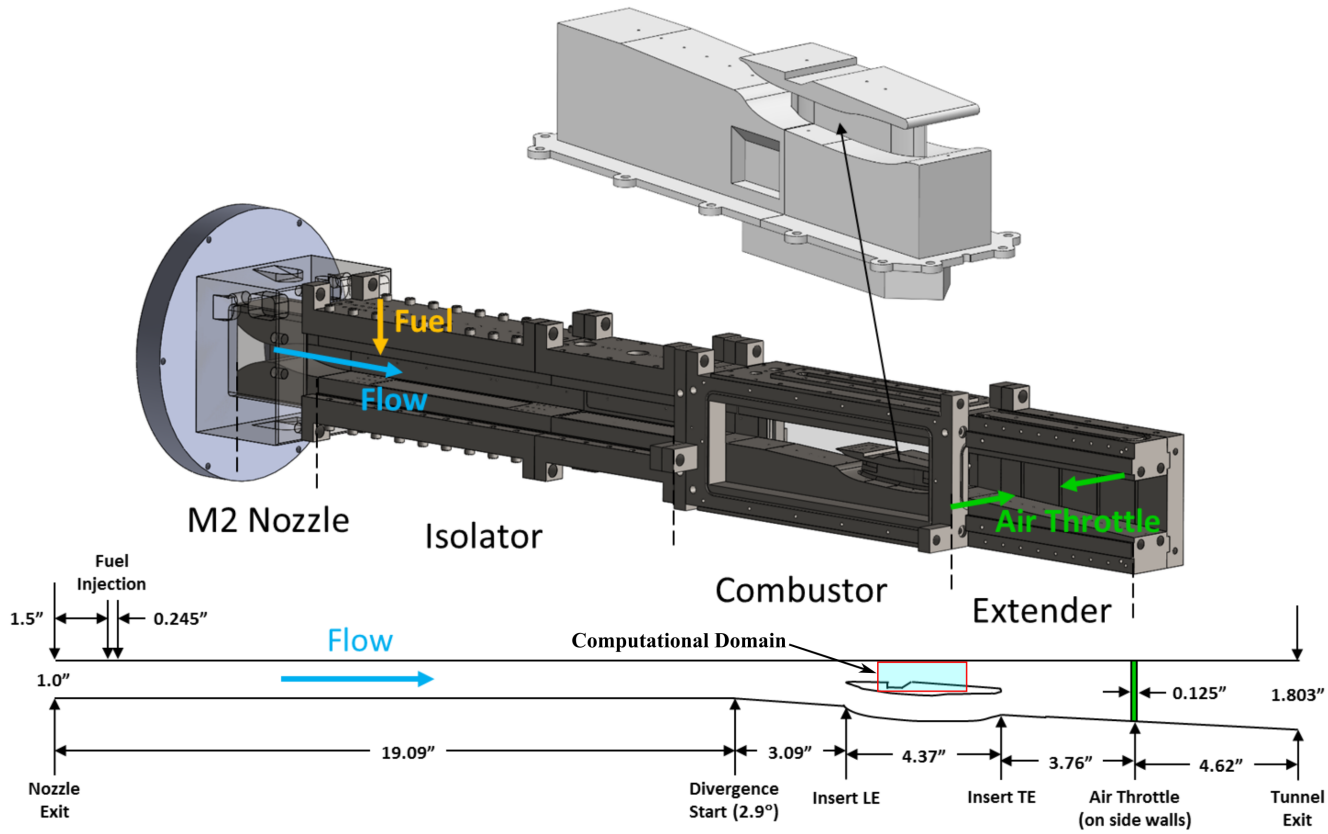

Figure 1: Experimental configuration at UVASCF. Full facility flowpath with cavity-ramp flameholder shown.

Sec. 6.

2 Experimental Configuration & Computational Geometry

Figure 1 shows the experimental configuration at the UVASCF. It is a direct-connect scramjet combustor that operates at Mach 5 enthalpy (total temperature of 1200 K). Eletrically-heated air flows through a Mach 2 nozzle into a constant-area isolator section. Ethylene is injected near the front of the isolator and the fuel-air mixture passes through a shock train that forms in the duct. The shock train can be controlled independently of the heat release in the combustor by modulating backpressure downstream of the combustor via an air throttle. The premixed fuel and air flows from the isolator into the combustor section. The cavity-ramp flameholder insert (top of Fig. 1) is placed into the combustor section with optical access for OH PLIF, PIV, and CARS diagnostics. The flameholder insert is 3D printed, three-part modular design with a hollow internal structure to allow for increased coolant flow.

The computational domain used in the simulations discussed in this paper is shown in Fig. 2. This domain is a 2D cross section through the center of the cavity flameholder insert, as indicated in Fig. 1. Initially, the domain is filled with a quiescent homogeneous mixture of ethylene and air with $\phi = 0.42$ at 1.72 atm and 1125 K. The Mach 0.6 inflow is at the same temperature and pressure. These conditions were chosen to reflect the conditions in a dual-mode combustor for a flight vehicle operating at Mach 5. At the end of the cavity combustor, the flow exhausts to a

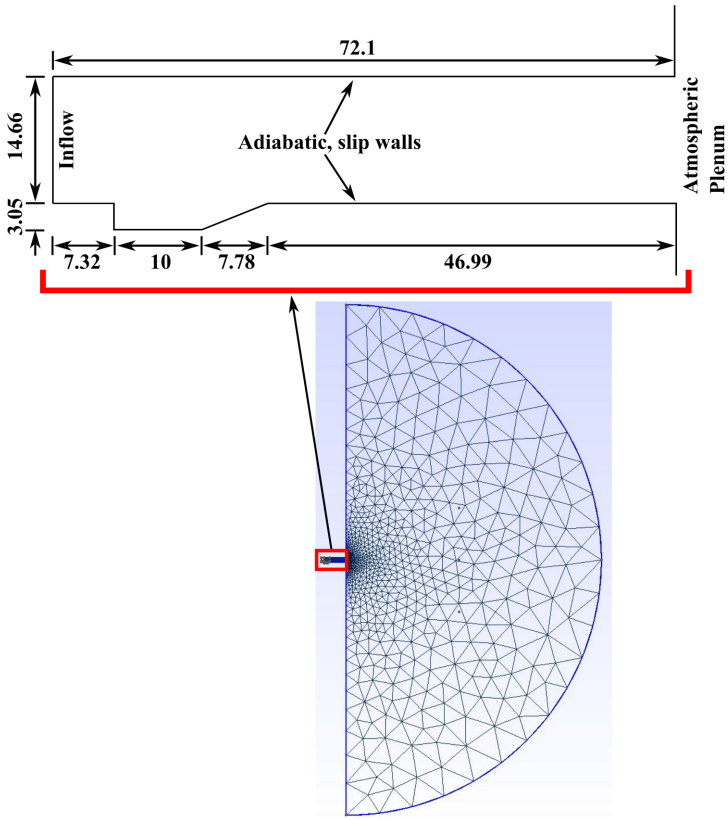

Figure 2: Computational domain. All dimensions in mm. Plenum radius is 168 mm.

large plenum with an outflow boundary condition of air at atmospheric temperature and pressure. Since it is assumed that the flow is slowed from a freestream condition of Mach 5 to a speed of Mach 0.6 in the combustor, the inflow temperature used in these simulations (1125 K) is nearly the stagnation temperature of the freestream flow (1200 K). The stagnation pressure losses associated with slowing the flow this drastically would likely prohibit operation of an actual propulsion system at these conditions, but it is an interesting case to study as it represents the lower operability limit of subsonic combustion in a Mach 5 dual-combustion engine. Future work will investigate higher flow speeds and lower inflow temperatures.

Experiments are ongoing to characterize flame structure and combustion efficiency as a function of fuel equivalence ratio, ϕ. Figure 3 shows natural luminosity images of the cavity-anchored flame for $\phi = 0.43$ and 0.36. In the more fuel-rich $\phi = 0.43$ case it is evident that the flame expands further vertically upward into the combustor than the leaner case.

3 Numerical Model

These simulations solve the unsteady, compressible Navier-Stokes equations for a chemically reacting gas:

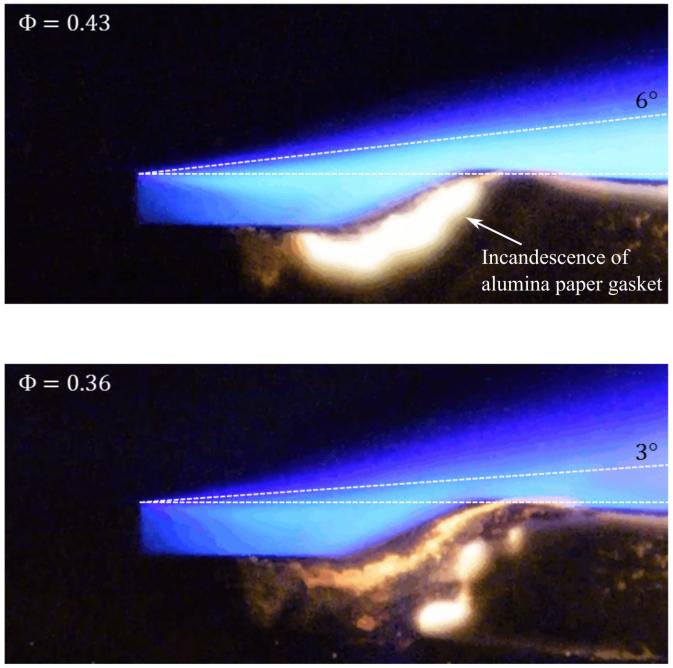

Figure 3: Natural luminosity images of the cavity-anchored flame at UVASCF for $\phi = 0.43$ and 0.36.

$$\frac{\partial \rho \mathbf{v}}{\partial t} + \nabla \cdot (\rho \mathbf{v} \otimes \mathbf{v}) = -\nabla p - \nabla \cdot \mathbb{T}(\mu, \nabla \mathbf{v}) \tag{1}$$

$$\begin{aligned} \frac{\partial \rho e_t}{\partial t} + \nabla \cdot ((\rho e_t + p)\mathbf{v}) &= \nabla \cdot \lambda \nabla T \\ &\quad - \nabla \cdot \sum_{k=1}^{N_s} h_k (\rho D_k \nabla C_k - D_k C_k \nabla \rho) \\ &\quad - \nabla \cdot (\mathbb{T}(\mu, \nabla \mathbf{v}) : \mathbf{v}) \end{aligned} \tag{2}$$

$$\frac{\partial C_k}{\partial t} + \nabla \cdot (C_k \mathbf{v}) = D_k \nabla C_k - D_k \frac{C_k}{\rho} \nabla \rho + \omega_k. \tag{3}$$

Density, pressure, and internal energy are calculated based on concentrations and mixture temperature by $\rho = \sum_{k=1}^{N_s} C_k W_k$, $p = R^o T \sum_{k=1}^{N_s} C_k$, and $e_t = u(C_k, T) + \frac{\mathbf{v} \cdot \mathbf{v}}{2}$ respectively. All transport quantities,D_k, λ, and μ, are evaluated as concentration based mixture-averaged quantities of polynomial fits based on temperature as provided by [14, 15, 16]. However, the polynomials were adjusted so that one 6th order polynomial, instead of two, can describe the thermodynamic state of each species within 0.01 percent accuracy of the SANDIA fits in temperature ranges 300 to 3000 K ensuring continuous differentiability in C^∞. This ensures differentiability for implicit methods that are currently under development. The reaction term, ω_k, is calculated using a time-split approach that supports implicit detailed chemical mechanism integration in time.

3.1 The Discontinuous Galerkin Discretization

Here we rewrite 1-3 in a more concise, flux-expression form, representation as

$$\frac{\partial \mathbf{y}}{\partial t} + \nabla \cdot \left(\mathcal{F}^c\left(\mathbf{y}\right) - \mathcal{F}^v\left(\mathbf{y}\right)\right) = \mathcal{S}\left(\mathbf{y}\right). \tag{4}$$

Where

$$\mathbf{y} = \begin{Bmatrix} \rho \mathbf{v} \\ \rho\left(u + \frac{\mathbf{v}\cdot\mathbf{v}}{2}\right) \\ C_k \end{Bmatrix} \tag{5}$$

$$\mathcal{F}^c = \begin{Bmatrix} \rho \mathbf{v} \otimes \mathbf{v} - p\mathbb{I} \\ \left(\rho e_t + p\right)\mathbf{v} \\ C_k \mathbf{v} \end{Bmatrix}, \tag{6}$$

$$\mathcal{F}^v = \begin{Bmatrix} \mathbb{T}\left(\mu, \nabla \mathbf{v}\right) \\ \lambda\left(C_k, T\right)\nabla T - \left(\mathbb{T}\left(\mu, \mathbf{v}\right) : \mathbf{v}\right) - \nabla \cdot \sum\limits_{k=1}^{N_s} h_k\left(\rho D_k \nabla C_k - D_k C_k \nabla \rho\right) \\ D_k \nabla C_k - D_k \frac{C_k}{\rho}\nabla \rho \end{Bmatrix}, \tag{7}$$

and

$$\mathcal{S}\left(\mathbf{y}\right) = \begin{Bmatrix} \mathbf{0} \\ 0 \\ \omega_k \end{Bmatrix} \tag{8}$$

The domain, Ω, is decomposed into non-overlapping finite elements and denoted as $\mathcal{T}_h$. The discrete space of discontinuous polynomials is then defined as, for $p \in \mathbb{N}$,

$$\mathbf{V}_h^p := \left\{\mathbf{v}_h \in \left[L^2\left(\Omega\right)\right]^d : \mathbf{v}_{h|\kappa} \in \left[\mathbb{P}_p(\kappa)\right]^d \forall \kappa \in \mathcal{T}_h\right\}, \tag{9}$$

We define the jump and average operators for vector valued functions

$$\{\{\mathbf{v}\}\} = \frac{1}{2}(\mathbf{v}^+ + \mathbf{v}^-) \text{ in } \Gamma_I, \qquad \{\{\mathbf{v}\}\} = \mathbf{v}^+ \text{ in } \Gamma,$$
$$[\![\mathbf{v}]\!] = (\mathbf{v}^+ \cdot \mathbf{n}^+ + \mathbf{v}^- \cdot \mathbf{n}^-) \text{ in } \Gamma_I, \qquad [\![\mathbf{v}]\!] = \mathbf{v}^+ \cdot \mathbf{n}^+ \text{ in } \Gamma,$$

for vector valued functions $\mathbf{v}_h \in \mathbf{V}_h^p$.

Following Hartmann and Leicht [17, 18], we arrive at the semi-discretization of Equation 4 in element based form, find $\frac{\partial \mathbf{y}_h}{\partial t} \in \mathbf{V}_h^p$ such that

$$\int_\Omega \frac{\partial \mathbf{y}_h}{\partial t} \cdot \mathbf{v}_h \,\mathrm{d}\mathbf{x} - \int_\Omega \left(\mathcal{F}^c(\mathbf{y}_h) - \mathcal{F}^v\left(\nabla \mathbf{y}_h\right)\right) : \nabla \mathbf{v}_h \,\mathrm{d}\mathbf{x} + \sum_{\kappa \in \mathcal{T}_h} \int_\Gamma \left(\hat{\mathbf{h}} - \hat{\sigma}_h \mathbf{n}\right) \cdot \mathbf{v}_h \,\mathrm{d}s$$
$$+ \sum_{\kappa \in \mathcal{T}_h} \int_\Gamma \left(\hat{\mathbf{y}}_h - \mathbf{y}_h\right) \otimes \mathbf{n} : \nabla \mathbf{v}_h \,\mathrm{d}s = \mathcal{S}\left(\mathbf{y}_h\right), \tag{10}$$

$\forall \mathbf{v}_h \in \mathbf{V}_h^p$ and $\hat{\mathbf{h}}$ is a consistent and conservative numerical flux associated with the convective operator. The numerical fluxes associated with the viscous operator, $\hat{\mathbf{y}}_h$ and $\hat{\sigma}_h$, are defined following [18] as

$$\hat{\mathbf{y}}_h = \{\{\mathbf{y}_h\}\}, \qquad \hat{\sigma}_h = \left(\left\{\left\{\mathcal{F}^v_{\nabla \mathbf{y}} \nabla \mathbf{y}_h\right\}\right\} - \eta \delta\left(\mathbf{y}_h\right)\right) \text{ in } \Gamma, \tag{11}$$

where η is a constant chosen such that stability is guaranteed. Artificial viscosity was used to smooth discontinuities and regions of high shear using the shock capturing explained by Hartmann [19]. The computational domain is discretized into tetrahedral elements. Element sizes range from 10 μm in the cavity to 300 μm in the center of the combustor outflow into the atmospheric plenum.

3.2 Temporal Integration

The semi-discrete equations are discretized in time using a Standard-Strong-Stability-Preserving-Runge-Kutta method[20]. The temporal integration of the non-stiff convection operators is separated from the temporal integration stiff source term via Strang operator splitting. The temporal integration of the chemical source term is done implicitly via finite elements. Second order accurate integration is used for the explicit integration and up to fourth order accurate integration is used for the chemical source term.

4 Results

4.1 Three Step Model

The first simulation performed solved the equations described in Sec. 3.1 with the three step, six species chemical model for ethylene-air combustion as described in [13]. Figure 4 shows contours of temperature and mass fraction of CO_2, Y_{CO2}, from 5.18 ms to 65 ms. The initial inflow of reactant from the left boundary compresses the quiescent reactant in the combustor, resulting in a compression wave propagating from left to right as shown at 5.18 ms. The compression wave is trailed by a rarefaction wave which forms as the temperature, pressure, and density, initially increased behind the compression wave, gradually equilibrate to match the incoming flow conditions. As the compression and rarefaction waves propagate past the cavity, a shear layer at the leading edge of the cavity results in the formation of a recirculation zone. This is first visible at 12.5 ms. The size of the vortex that forms in the cavity increases as it pulls in the high temperature reactant that is trailing the compression wave.

The ethylene and air mixture reaches a sufficient temperature for autoignition just upstream of the rarefaction wave, as shown at 19.1 ms. The temperature, pressure, and density of the reactant are increased by the initial compression wave. The reactant is then further compressed by the reflection of additional pressure waves against the cavity ramp. As a result, the highest temperatures in the combustor are observed on the high-temperature side of the rarefaction wave and this is where autoiginition is first observed. Autoiginition also occurs in the cavity as the high temperature reactant is pulled into the recirculation zone. The initial locations of autoignition are marked at 19.1 ms in the Y_{CO2} plot.

By $\sim$50 ms, several flamelets have ignited in the cavity. As time progresses, the flamelets coalesce into a cavity-stabilized flame recirculating just downstream of the leading edge of the cavity. Figure 5 shows temperature, Y_{CO2}, and Mach number contours of the cavity-stabilized flame at 100.8 ms. Combustion occurs primarily in the vortex generated by the recirculation in the cavity, with small flamelets continuing to burn downstream of the ramp. Local velocity decreases in the cavity as the burning gas recirculates, and then increases as the gas exits the cavity and travels into the constant-area region of the combustor. Mach number near the combustor outflow rises to nearly sonic as the gas accelerates and the local speed of sound decreases due to decreasing temperature.

4.2 117 Step Model

Figure 6 shows a cavity-stabilized flame, simulated with the 117 step chemical model, at approximately the same instant in time ($\sim$100 ms) as the results shown in Fig. 5 for the three step model. There is significant recirculation in the cavity, as shown in the x-velocity, V_{x}, contours. Velocity increases towards the outflow of the combustor as the flame expands upward into the center of the domain. The flame is anchored to the cavity lip and the gas in the cavity is entirely combustion

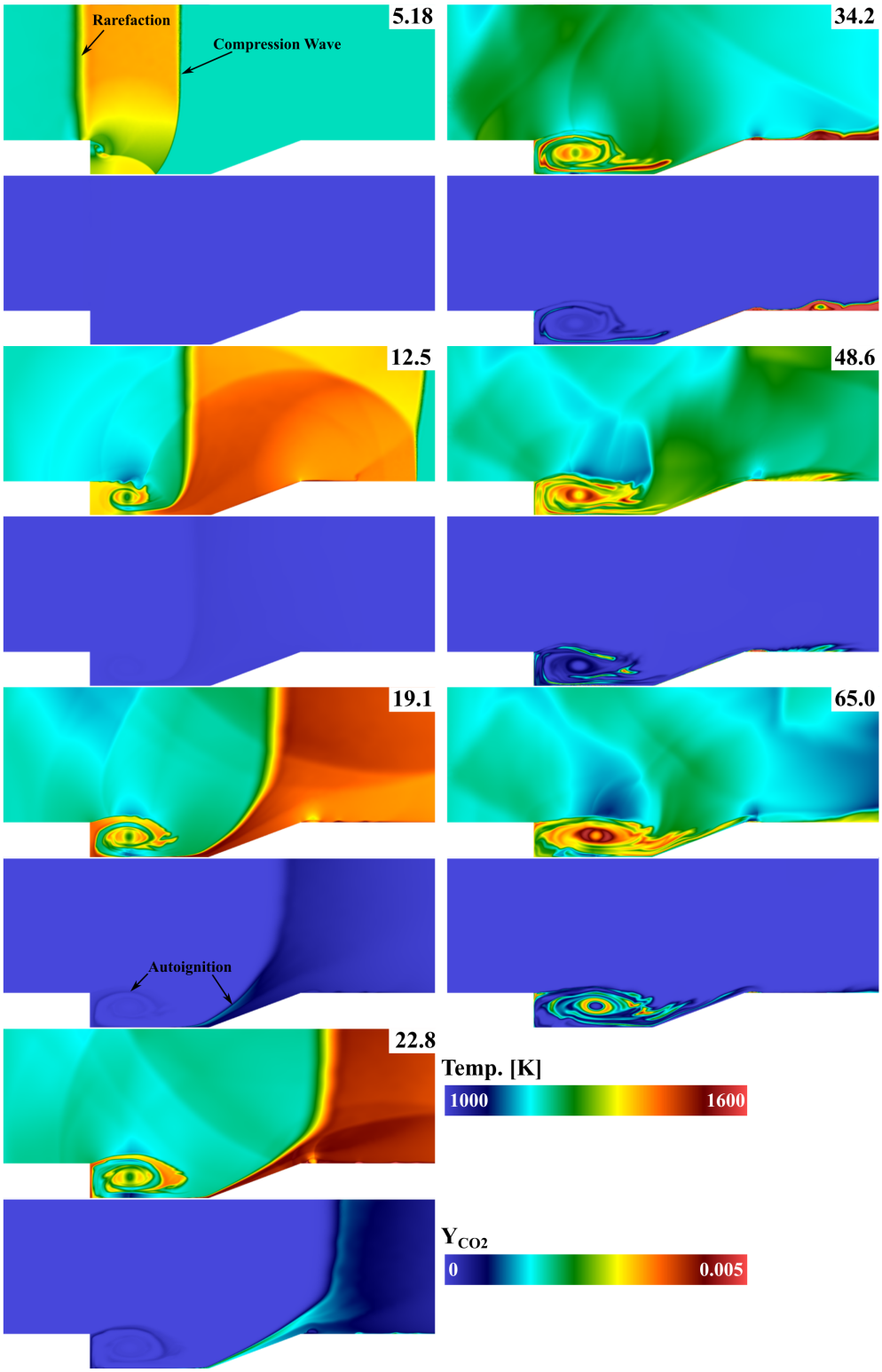

Figure 4: Temperature and mass fraction of CO_2 showing autoignition in the three-step model case. Time is shown in ms in the frame corners. Domain is x =[3 mm, 38.1 mm] and y = [-3.048 mm, 14.66 mm].

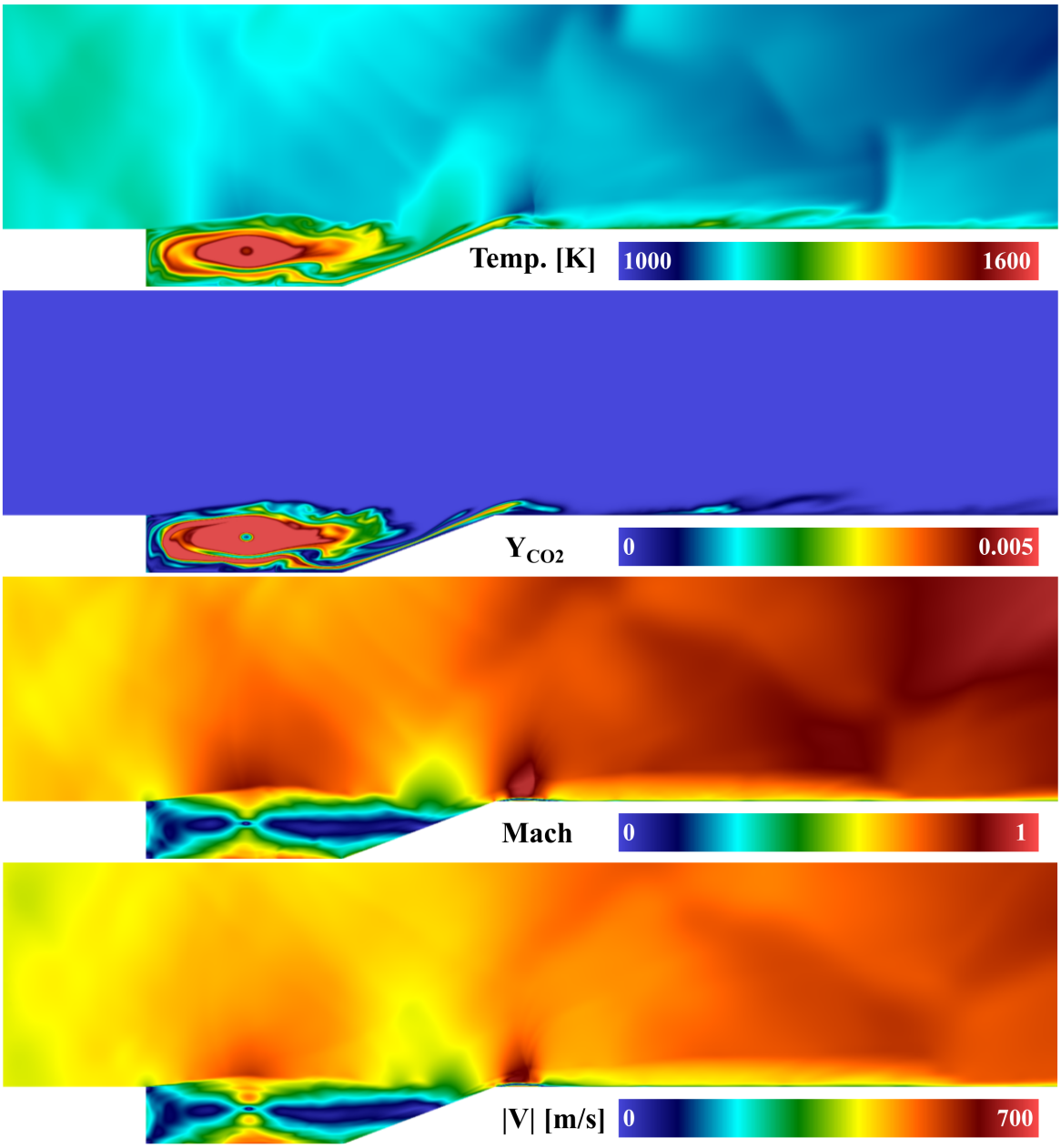

Figure 5: Temperature, mass fraction of CO_2, Mach number, and velocity magnitude at 100.8 ms with the three step chemical model. Domain shown is x =[0 mm, 72.1 mm] and y = [-3.048 mm, 14.66 mm].

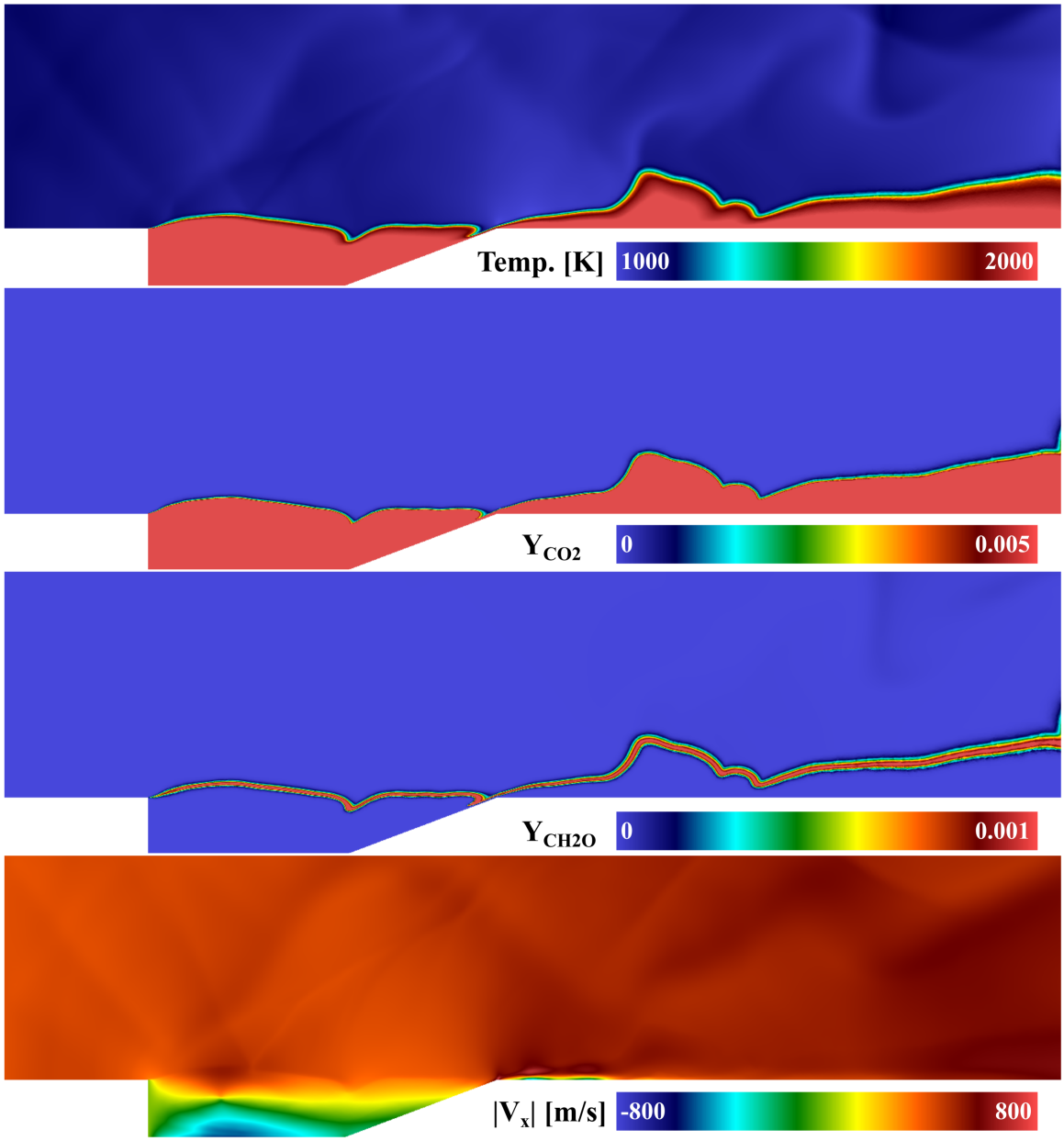

Figure 6: Temperature, mass fraction of CO_2, mass fraction of CH_2O, and x-velocity at 104.8 ms with the 117 step chemical model. Domain shown is x =[0 mm, 72.1 mm] and y = [-3.048 mm, 14.66 mm].

products. This is evident in the Y_{CO2} plot. The formaldehyde mass fraction, Y_{CH2O2}, contours show the flame location. Combustion occurs across a thin region of gas, beginning at the cavity lip and extending over the top of the cavity into the combustor outflow. Formaldehyde mass fraction was chosen to show the flame location because it is a minor species in the reaction chain and is only visible in a thin layer at the flame surface. Additionally, it can be measured spatially in the experimental facility for comparison to simulation results.

5 Discussion

Comparison of the simulation results at 100 ms between the three and 117 step models, Figs. 5 and 6, respectively, shows significant differences in flame structure between the two cases. In the case of the three step model, combustion occurs almost exclusively within the cavity and the reactant that is not drawn into the recirculation zone flows over the cavity and out of the combustor without chemical reactions occurring. The flame is not anchored directly to the cavity lip, but is revolving in a vortex within the cavity. It is expected that the combustor efficiency in this simulation is much lower than that in the experiment.

In the case of the 117 step model, the combustor appears to operate much more efficiently. The flame is anchored to the cavity lip and extends over and past the cavity toward the combustor outflow. The flame also expands toward the center of the cavity as it approaches the outflow. More of the reactant is converted to product in this case than with the three step model. When comparing the simulation results to the chemiluminescence images from the experiment with $\phi = 0.43$, shown in Fig. 3, it is evident that the accuracy in the chemical model is crucial to performing simulations that reflect the experimental conditions at UVASCF. The results with the 117 step model show good agreement with the experimental results. In both this simulation and in the experiment, the flame is anchored to the cavity lip and it continues to expand toward the center of the combustor downstream of the ramp.

Despite the differences between the two simulation cases, the autoignition of the reactant in the recirculation zone and across the rarefaction wave was observed to be independent of the chemical model. This indicates that both chemical models have sufficient fidelity to accurately simulate the autoignition process of the ethylene-air mixture. Additional cases were run where the gas everywhere in the domain is initialized to be moving with the same velocity as the inflowing gas; in these cases, no initial compression and rarefaction waves were formed and autoignition did not occur. Once the non-reacting flow reached a relative steady-state solution, the reactant was ignited by initiating a small, high-temperature region just downstream of the cavity lip to simulate spark ignition. In these cases, the same flame structure formed that is shown in Figs. 5 and 6. Thus, the flame structure was observed to be independent of the method of ignition.

The simulations discussed in this paper used slip walls and a laminar inflow and thus do not reflect the turbulent inflow conditions to the combustor in the UVASCF facility. It is likely that the boundary layers and turbulence in the experimental combustor lead to increased diffusion and more complete combustion than we observe in the simulations. Future work will use no-slip walls and turbulent inflow conditions based on measured turbulence levels in the facility to accurately reflect the combustor inflow conditions. A wall temperature will be assigned based on experimental measurements. Additionally, a three-dimensional domain will be used to capture the full effects of turbulence on the combustion process.

6 Conclusions

This report summarizes the early phases of an effort to apply a high-fidelity Discontinuous-Galerkin code, JENRE, and finite-rate, multi-step chemical models to accurately and efficiently simulate the complex reactive flow in the University of Virginia Supersonic Combustion Facility. The experimental capabilities of the facility are relevant to the Navy as interest increases in airbreathing propulsion systems for hypersonic vehicles. The facility is capable of testing combustors for dual-mode scramjets at flight enthalpies up to Mach 5. In the configuration studied in this work, ethylene is injected upstream of the combustor, in the scramjet isolator, such that the flow into the combustor is a relatively homogeneous mixture of ethylene and air. Mixing of the fuel and air upstream of the combustor allows for shorter combustor lengths and potentially more efficient and complete combustion, but the effectiveness of this design requires additional computational and experimental study.

In this work, we concentrate on ramjet operation of the dual-mode combustor at a freestream Mach number of 5 and combustor inflow Mach number of 0.6. Slowing the flow to this low Mach number prior to combustion will likely result in high pressure drag within the engine. This lower limit of the engine operational range warrants further study, particularly into the stability and efficiency of the combustor in this low-subsonic combustion mode. Two simulations were discussed in this paper, one using a three step, six species chemical model and the other using a 117 step, 26 species model for ethylene-air combustion. In both cases, a cavity-stabilized flame forms after autoignition of the reactant. The flame structure differed significantly depending on the chemical model used. With the three step chemical model, a swirling flame develops in the recirculation zone within the cavity and no combustion occurs downstream of the cavity. With the 117 step model, the flame is anchored to the cavity lip and extends over the cavity and into the combustor outflow. The results with the 117 step model indicate more complete combustion of the premixed reactant and show better agreement with experimental results.

Future work will replicate the turbulence levels in the combustor measured in the experimental facility and simulate the flow through the full three-dimensional domain with the 117 step chemical model. It is expected that these results will show excellent agreement with experiments, based on the qualitative similarities in flame structure observed between the experiment and the simulations discussed in this report using a two-dimensional domain and laminar inflow boundary conditions. Further computations will be performed with a supersonic inflow to simulate the combustor conditions during scramjet operation.

References

[1] Ben-Yakar, A. and Hanson, R. K., "Cavity flame-holders for ignition and flame stabilization in scramjets: an overview," *Journal of propulsion and power*, Vol. 17, No. 4, 2001, pp. 869–877.

[2] Yu, K. H., Wilson, K. J., and Schadow, K. C., "Effect of flame-holding cavities on supersonic-combustion performance," *Journal of Propulsion and Power*, Vol. 17, No. 6, 2001, pp. 1287–1295.

[3] Wang, Z., Wang, H., and Sun, M., "Review of cavity-stabilized combustion for scramjet applications," *Proceedings of the Institution of Mechanical Engineers, Part G: Journal of Aerospace Engineering*, Vol. 228, No. 14, 2014, pp. 2718–2735.

[4] Mathur, T., Gruber, M., Jackson, K., Donbar, J., Donaldson, W., Jackson, T., and Billig, F., "Supersonic combustion experiments with a cavity-based fuel injector," *Journal of Propulsion and Power*, Vol. 17, No. 6, 2001, pp. 1305–1312.

[5] Rockwell, R. D., Goyne, C. P., Chelliah, H., McDaniel, J. C., Rice, B. E., Edwards, J. R., Cantu, L. M., Gallo, E. C., Cutler, A. D., and Danehy, P. M., "Development of a Premixed Combustion Capability for Dual-Mode Scramjet Experiments," *Journal of Propulsion and Power*, 2017, pp. 1–11.

[6] Geipel, C. M., Rockwell, R., Chelliah, H., Cutler, A. D., Spelker, C., Hashem, Z., and Danehy, P. M., "High-Spatial-Resolution OH PLIF Visualization in a Cavity-Stabilized Ethylene-Air Turbulent Flame," *33rd AIAA Aerodynamic Measurement Technology and Ground Testing Conference*, 2017, p. 3901.

[7] Kirik, J. W., Goyne, C. P., McDaniel, J. C., Rockwell, R. D., Cantu, L. M., Gallo, E. C., and Cutler, A. D., "Aerodynamic Characterization of a Cavity Flameholder in a Premixed Dual-Mode Scramjet," *Journal of Propulsion and Power*, 2017, pp. 1–11.

[8] Cutler, A. D., Gallo, E. C., Cantu, L. M., Rockwell, R. D., and Goyne, C. P., "Coherent anti-Stokes Raman spectroscopy of a premixed ethylene–air flame in a dual-mode scramjet," *Combustion and Flame*, Vol. 189, 2018, pp. 92–105.

[9] Ramesh, K. K., Edwards, J. R., Goyne, C. P., and McDaniel, J. C., "Large Eddy Simulation of High-Speed, Premixed Ethylene Combustion," *53rd AIAA Aerospace Sciences Meeting*, 2015, p. 0356.

[10] Nielsen, T., Edwards, J. R., Chelliah, H. K., Lieber, D., Goyne, C. P., Rockwell, R. D., and Cutler, A. D., "Hybrid LES/RANS Simulation of Supersonic Premixed Ethylene Combustion," *2018 AIAA Aerospace Sciences Meeting*, 2018, p. 1145.

[11] Rauch, A. H., Konduri, A., Chen, J., Kolla, H., and Chelliah, H. K., "DNS Investigation of Cavity Stabilized Premixed Turbulent Ethylene-Air Flame," *2018 AIAA Aerospace Sciences Meeting*, 2018, p. 1674.

[12] Wang, H., Dames, E., Sirjean, B., Sheen, D., Tangko, R., Violi, A., Lai, J., Egolfopoulos, F., Davidson, D., Hanson, R., et al., "A high-temperature chemical kinetic model of n-alkane (up to n-dodecane), cyclohexane, and methyl-, ethyl-, n-propyl and n-butyl-cyclohexane oxidation at high temperatures," *JetSurF version*, Vol. 2, No. 2, 2010, pp. 19.

[13] Baurle, R., Mathur, T., Gruber, M., and Jackson, K., "A numerical and experimental investigation of a scramjet combustor for hypersonic missile applications," *34th AIAA/ASME/SAE/ASEE Joint Propulsion Conference and Exhibit*, 1998, p. 3121.

[14] Kee, R. J., Grcar, J. F., Smooke, M. D., Miller, J., and Meeks, E., "PREMIX: a Fortran program for modeling steady laminar one-dimensional premixed flames," *Sandia National Laboratories Report*, , No. SAND85-8249, 1985.

[15] Kee, R. J., Rupley, F. M., Meeks, E., and Miller, J. A., "CHEMKIN-III: A FORTRAN chemical kinetics package for the analysis of gas-phase chemical and plasma kinetics," *Sandia national laboratories report SAND96-8216*, 1996.

[16] Goodwin, D. G., Moffat, H. K., and Speth, R. L., "Cantera: An Object-oriented Software Toolkit for Chemical Kinetics, Thermodynamics, and Transport Processes," http://www.cantera.org, 2017, Version 2.3.0.

[17] Hartmann, R., "Adjoint consistency analysis of discontinuous Galerkin discretizations," *SIAM Journal on Numerical Analysis*, Vol. 45, No. 6, 2007, pp. 2671–2696.

[18] Hartmann, R. and Leicht, T., "Higher order and adaptive DG methods for compressible flows," *VKI LS 2014-03: 37th Advanced VKI CFD Lecture Series: Recent developments in higher order methods and industrial application in aeronautics, Dec. 9-12, 2013*, edited by H. Deconinck, Von Karman Institute for Fluid Dynamics, Rhode Saint Genèse, Belgium, 2014.

[19] Hartmann, R., "Adaptive discontinuous Galerkin methods with shock-capturing for the compressible Navier–Stokes equations," *International Journal for Numerical Methods in Fluids*, Vol. 51, No. 9-10, 2006, pp. 1131–1156.

[20] Gottlieb, S., Shu, C., and Tadmor, E., "Strong stability-preserving high-order time discretization methods," *SIAM review*, Vol. 43, No. 1, 2001, pp. 89–112.